Clay Minerals (2025), **60**, 307–322
doi:10.1180/clm.2025.10018

Article

Investigation of iron/bentonite interaction based on powdered mixtures

Stephan Kaufhold[1], Kristian Ufer[1], Reiner Dohrmann[1,2], Franz Renz[3], René Lucka[3], Maximilian Seydi Kilic[3] and Sven Krüger[4]

[1]BGR, Bundesanstalt für Geowissenschaften und Rohstoffe, Hannover, Germany; [2]LBEG, Landesamt für Bergbau, Energie und Geologie, Hannover, Germany; [3]Leibniz Universität Hannover, Institut für Koordinationschemie, Hannover, Germany and [4]Theoretische Chemie, Technische Universität München, Garching, Germany

Abstract

To date, published studies have proven that the reactions at the iron/bentonite interface are complex and only partly understood. In the present study, mixtures of bentonite powder and iron powder were prepared, which allowed for varying individual parameters. The results confirmed some controversial previously reported conclusions and revealed new findings. More specifically, Na-exchanged samples showed a reduced extent of corrosion compared to Ca/Mg-exchanged ones, and the addition of reactive silica increased the extent of corrosion, which has not been reported to date. The negative temperature effect (less corrosion at higher temperatures), which was reported previously, could only be confirmed for Ca/Mg-bentonites. One Na-bentonite showed the opposite effect, but this sample also contained reactive silica in contrast to the others. The present study proves for the first time that the type of exchangeable cation can affect the type of corrosion product, which could be an explanation for why the 7 Å corrosion product was not reported in all corrosion tests (sometimes only magnetite was reported). In addition, experiments that ran for 36 months showed that the corrosion progress of six different bentonites was different. Three bentonite/iron mixtures did not show progress in corrosion after 12 months, whereas the other three showed ongoing corrosion. Using the former three bentonite/iron mixtures would significantly increase high-level radioactive waste canister lifetime, but future work should be devoted to the identification of the reason for this differing long-term performance, differing thermal behaviour and differing corrosion products resulting from different types of exchangeable cation.

Keywords: Bentonite alteration; interlayer cation population; iron/bentonite interaction; iron corrosion

(Received 4 August 2025; revised 4 November 2025; accepted 11 November 2025; Accepted Manuscript online: 27 November 2025)

Bentonites are candidate materials for the isolation of metal canisters containing high-level radioactive waste (HLRW). A bentonite barrier will be used in the case of crystalline host rocks, as these are often fractured. However, even in some clay host rock-based repositories, bentonite will also be used as an additional barrier (e.g. in Switzerland; Sellin & Leupin, 2013). The metal canister containing the HLRW represents an important barrier at all stages, particularly during heat development in the early phase. The canister will be in contact either with clay stone or even more often with bentonite. Only in cases of a supercontainer, such as will be used in Belgium, is there no contact between the waste canisters and clay. In the Swedish KBS-3 concept, copper will be used as a canister material, as it did not show any specific corrosion reactions in laboratory experiments with sulfide-free bentonites (Kosec *et al.*, 2015; Kaufhold *et al.*, 2017). Most concepts, however, favour iron or carbon steel as canister materials, such as in Switzerland, France, Japan, Belgium and Spain (Mota-Heredia *et al.*, 2023). In contrast to copper, specific reactions of iron and bentonite under anaerobic conditions (which are expected in a repository) have been identified. The transition from the initial aerobic to anaerobic conditions was recently discussed by Kiczka *et al.* (2024). Corrosion will reduce the thickness of the metal canister wall and also affect the smectites (e.g. Zandanel *et al.*, 2022; Sun *et al.*, 2023). The current understanding of the alteration reactions was recently summarized by Wilson *et al.* (2025) focusing on modelling the iron/bentonite interaction. These authors also state that 'uncertainties remain', probably resulting from the 'many potential complex couplings' in the iron/bentonite system, such as that investigated in the present study. In addition, little information is available regarding Fe-admixtures such as carbon (C) in carbon steel. Kaufhold *et al.* (2025) compared bentonite/metal interactions with different iron-based alloys containing various carbon contents and particle/crystallite sizes. No significant differences in the corrosion rates of iron-based alloys with various carbon contents and particle/crystallite sizes were observed. Different results, however, were published with respect to the corrosion products of iron-based alloys. Most studies agree that magnetite forms (Martin

Corresponding author: Stephan Kaufhold; Email: s.kaufhold@bgr.de

Cite this article: Kaufhold S, Ufer K, Dohrmann R, Renz F, Lucka R, Kilic MS and Krüger S (2025) Investigation of iron/bentonite interaction based on powdered mixtures. *Clay Minerals* **60**, 307–322. https://doi.org/10.1180/clm.2025.10018

© The Author(s), 2025. Published by Cambridge University Press on behalf of The Mineralogical Society of the United Kingdom and Ireland. This is an Open Access article, distributed under the terms of the Creative Commons Attribution licence (http://creativecommons.org/licenses/by/4.0), which permits unrestricted re-use, distribution and reproduction, provided the original article is properly cited.

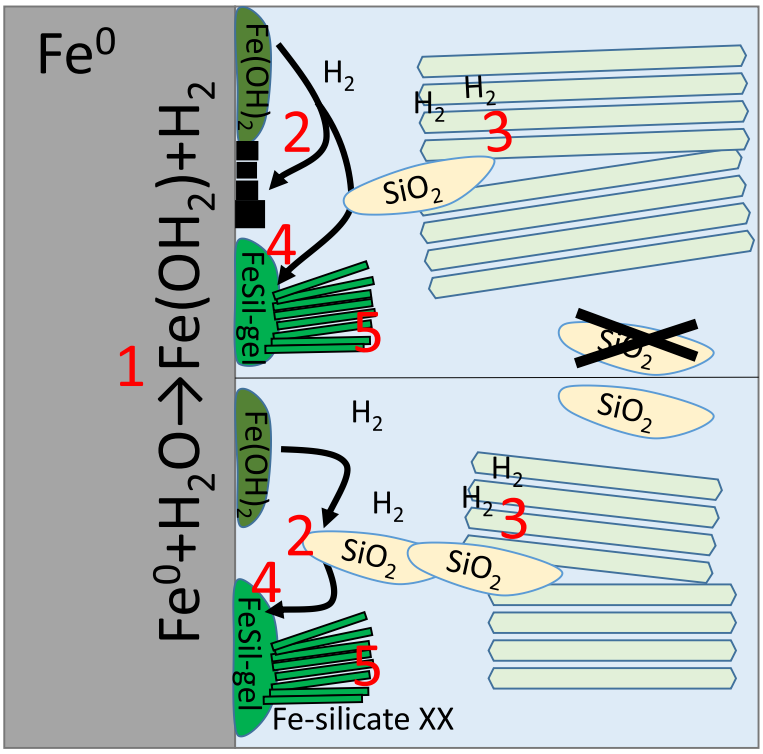


Figure 1. Schematic representation of the iron/bentonite reactions identified to date based on Kaufhold *et al.* (2020a), not considering the presence of sulfides, carbonates and/or HCO_3^-. Two scenarios are distinguished: upper part = no reactive silica present from the beginning onwards; lower part = some reactive silica naturally present in the bentonite from the beginning onwards. See main text for details of the red numbers.

et al., 2008; Osacky *et al.*, 2010), but different iron silicates were also observed (Lantenois *et al.*, 2005; Lanson *et al.*, 2012; Kaufhold *et al.*, 2015, 2020b). According to Lantenois *et al.* (2005), the type of corrosion product depends on the composition of the smectite, pH, exchangeable cation and temperature. At temperatures <100°C, 1:1 iron-layered silicates (7 Å phases) form, whereas 2:1 iron-layered silicates (14 Å phases) were found at higher temperatures (Lantenois *et al.*, 2005). Lanson *et al.* (2012) provided an in-depth study on the characterization of the corrosion products and identified cronstedtite and odinite, both Fe-dominated 1:1-layer silicates. The anaerobic corrosion mechanism, however, is still under discussion. Kaufhold *et al.* (2020a) proposed a reaction mechanism that is in accordance with many previous studies and is illustrated in Fig. 1:

(1) Reduction of water (formation of H_2) and formation of a ferrous iron gel (Lee *et al.*, 2006; Stoulil *et al.*, 2013; Kaufhold *et al.*, 2020a). This reaction takes place as soon as water comes into contact with an iron surface under anaerobic conditions (whether or not bentonite is present).
(2) The ferrous iron gel either recrystallizes into magnetite (Schikorr, 1933; Lee *et al.* 2006) or reacts with Si^{4+}, forming an iron silicate (gel) if Si is available in the system from the beginning onwards (Kaufhold *et al.*, 2020b).

These first two steps explain why magnetite is often observed to be the first layer. Depending on the chemical composition of the bentonite and the fluid, different types of corrosion products form on the outer surface. Most often iron silicates (as highlighted earlier) and carbonates have been reported (Savoye *et al.*, 2001; Martin *et al.*, 2008; Romaine *et al.*, 2013; El Mendili *et al.*, 2014). In the presence of sulfides (and bacteria), even iron sulfides have been observed (El Mendili *et al.*, 2015; Schlegel *et al.*, 2018). According to Kaufhold *et al.* (2020b) and Rivard *et al.* (2015), so-called reactive silica (poorly ordered SiO_2 phases such as cristobalite or opal) affect the reaction pathway, as elucidated in Fig. 1.

(3) The structural Fe^{3+} of smectites is reduced by H_2 (Didier *et al.*, 2012; Kaufhold *et al.*, 2015), which increases the solubility of smectites (reductive dissolution; Drits & Manceau, 2000; Jaisi *et al.*, 2005), adding Al^{3+} and Si^{4+} to the solution.

Some studies claim that the pH increases in such a way that smectite solubility is increased significantly, but Kaufhold *et al.* (2021) and Bildstein *et al.* (2006) found pH values of ~11, which would not be high enough to explain significant increases in smectite dissolution. In combination with reductive dissolution, however, a pH value of 11 could even further increase smectite solubility. This needs to be investigated in more detail in future.

(4) Iron silicates may form from a precursor silicate gel (Jullien *et al.*, 2005; Lanson *et al.*, 2012; Kaufhold *et al.*, 2020b) or even from the ferrous hydroxide if Si is available from the beginning onwards.
(5) The type of iron silicate that might form is known to depend on the ambient conditions (Lantenois *et al.*, 2005; also highlighted earlier).

The entire reaction (steps 1–4) is supposed to proceed as long as H_2 is consumed by the Fe^{3+} reduction because otherwise (without bentonite) iron in that system would become stable against oxidation (without bentonite, a black crust forms, but corrosion does not proceed). In this view, and considering Gorski *et al.* (2013), the corrosion is possibly determined by the redox-buffering capacity of bentonite, which is supposed to result from the fact that the structural Fe^{3+} in smectites can be reduced at different Eh values (depending on the bentonite). This effect can be understood on the

https://doi.org/10.1180/clm.2025.10018 Published online by Cambridge University Press

basis of energetic calculations (S. Krüger *et al.*, unpublished data, 2025), which indicate that Fe^{3+} in smectites is more easily reduced (at higher redox potential) if the distance to the next Mg atom in the octahedral sheet of the crystal structure is greater (which statistically increases in low-charged smectites with less octahedral Mg substitution). The *ab initio* density functional calculations proved that Fe^{2+} near to another bivalent cation such as Mg^{2+} in the octahedral sheet is much less favourable from an energetic point of view compared to Fe^{3+}, which is abundant in common smectites and only weakly repelled by Mg^{2+}. On the other hand, Fe^{2+} can be more easily accommodated in the octahedral sheet if other bivalent cations (Mg^{2+} or Fe^{2+}) are farther away (which is more often the case in low-charged smectites containing less Mg). Based on these calculations it was concluded that Fe^{3+} can be more easily reduced in low-charged smectites compared to high-charged ones containing more Mg.

Most of the likely parameters potentially affecting the corrosion extent have been identified in laboratory experiments, but they are sometimes discussed under a state of controversy. As an example, Lantenois *et al.* (2005) reported higher corrosion rates in the case of Na^+ as an exchangeable cation. Kaufhold *et al.* (2015) compared 38 Ca- and Na-exchanged bentonites with each other and with the same bentonites containing their natural cation populations. They concluded that the corrosion rate (extent of corrosion) decreases with the increasing portion of exchangeable Na^+ and increasing layer charge density (LCD). Lantenois *et al.* (2005) and Osacky *et al.* (2010) reported higher corrosion rates of bentonites rich in structural Fe, and Perronet *et al.* (2007) assumed that crystal edges play an important role in this. Stoulil *et al.* (2013) reported lower corrosion rates at higher temperatures, which was explained by the denser magnetite layer that forms at higher temperatures leading to less diffusion of Fe through this layer. In addition, Battallion *et al.* (2010) concluded that the corrosion rate is determined by the diffusion of Fe^{2+} through the magnetite layer. The presence of reactive silica (e.g. opal-A or finely ground quartz) was found to determine the corrosion pathway (Rivard *et al.*, 2015), but no information is available regarding its effect on the corrosion rate/extent of corrosion. The same holds true for carbonate minerals and/or the presence of HCO_3^--containing waters. Notably, all of these tests were conducted with higher water contents than expected at the real metal/bentonite interface. The water content can, however, be kept as low as possible to provide homogeneous mixtures (gels) and at the same time be close to real conditions.

The aims of the present study are to (1) establish a method that is suitable for comparing the extent of corrosion of various bentonite/iron mixtures and (2) quantify the effect of the aforementioned parameters (type of exchangeable cation, availability of reactive silica, time, temperature, iron particle size) on the extent of corrosion.

Materials and methods

Materials

Kaufhold *et al.* (2015) determined corrosion rates based on the mass loss of iron pellets exposed to bentonite gels. This method is tedious because several small pellets have to be used to increase the mass loss through a higher surface area so as to improve reproducibility, and these pellets all have to be picked out of the bentonite gel in its box. Moreover, a dense corrosion layer may form that cannot be removed by washing, hence affecting the gravimetric results. In the present study, bentonite powder, opal-A and iron powder were mixed (as reported by Guilliaume *et al.*, 2003). The iron powder cannot be separated quantitatively after the test, but the products can be investigated by bulk methods such as Mössbauer spectroscopy, X-ray diffraction (XRD) and thermal analysis. A comprehensive characterization of all bentonite samples is provided by Chiou *et al.* (2025), and selected parameters are summarized in Table 1. Some samples were selected because they are well-known HLRW bentonite references (e.g. MX80, BCV, FEBEX). Wyoming-type bentonites such as MX80 have been investigated by Svensk Kärnbränslehantering (SKB) for decades (e.g. Jacobsson & Pusch, 1978; Neretnieks, 1978; Pusch, 2002) and have been used by many other researchers as well. In contrast, the BCV bentonite was only recently envisaged as a reference bentonite for research by Správa Úložišť Radioaktivních Odpadů (Czech Radioactive Waste Repository Authority; SURAO), and hence less information is available regarding this material (Červinka *et al.*, 2018; Hausmannová *et al.*, 2018). The FEBEX bentonite was used to setup the FEBEX experiment, and it has been described by, for example, Fernandez *et al.* (2001, 2018). The other bentonites listed in Table 1 were selected because they performed differently in previous corrosion experiments. As an example, B36 was found to be more corrosive in six iron/bentonite corrosion experiments (except for KO4) in contrast to B6 (Kaufhold *et al.*, 2015). All samples are bentonites containing dioctahedral smectites. The samples were used as bulk material without any particle-size fractionation. They were dried at 60°C for 72 h and ground using a hammer mill. Selected Ca/Mg-bentonites were cation exchanged by Na^+. First, all carbonates were dissolved using a Na-acetate/acetic acid solution to avoid any re-exchange caused by partial calcite solution. Afterwards, samples were washed two times with NaCl (100-fold excess of Na^+ over the cation-exchange capacity (CEC)). Before drying and grinding, the samples were dialyzed to remove excess salt. The procedure is explained in detail by Kaufhold (2025), along with an in-depth characterization of all bentonites.

The content of soda-soluble silica (SSS), which is determined by soda extraction based on Kaufhold *et al.* (2008b), is used to characterize the amount of low-crystalline silica in the bentonites. Using the standard protocol yielded 90 mass% SSS for the opal-A sample (Table 1).

Corrosion tests

The extent of the iron/bentonite reaction can be determined based on various parameters such as the gravimetrical mass loss of the iron pellets, the extent to which structural Fe^{3+} is reduced, the amount of H_2 produced and the extent of secondary-phase formation (Kaufhold *et al.*, 2020a). In the present study, comparative tests with iron powder/bentonite mixtures were performed, which were assessed based on the extent to which the iron content decreased (expressed as the ratio of native iron after the test to total iron).

Standard tests were conducted using 3.0 g of clay (dried at 60°C for at least 3 days in an oven) mixed with 3.0 g of iron powder (–20 mesh, >99.5% Fe, purchased from Alfa Aesar/Thermo Scientific, Chemical Abstract Service (CAS): 7439-89-6) and 6 mL αwater (standard solid/liquid ratio = 1). Based on XRD results, the Fe powder consisted of α-iron. In the present study, all iron reactions are based on reactions with α-iron, and hence this is simply referred to as 'iron'. In many large-scale *in situ* tests in hard rock laboratories such as that in Äspö, Sweden, carbon steel was used, and it cannot be excluded that the carbon component may also be involved in certain reactions such as gas formation. The aim of the present

https://doi.org/10.1180/clm.2025.10018 Published online by Cambridge University Press

https://doi.org/10.1180/clm.2025.10018 Published online by Cambridge University Press

Table 1. List of samples, including some basic parameters and the times of the corrosion tests conducted. The LCD of all bentonites was calculated using the alkylammonium method except for B72, which was determined using the structural formula method and recalculated to alkylammonium method evaluated according to Kaufhold *et al.* (2011). Kaufhold *et al.* (2024) investigated the exchangeable cation population of the BCV used to set up the HotBENT project (which was from a different charge and hence is not given in the table) and found <2 meq 100 g^{-1} Na^{+}, ~42 meq 100 g^{-1} Mg^{2+} and 28 meq 100 g^{-1} Ca^{2+}. The XRD traces of opal-A and Fe^{0} can be found in the Fig. S1.

		B33, MX80	B19, FEBEX	B72, BCV	B6	B25	B36	Opal-A, silica gel, cat litter	Fe^{0}, iron, Alfa Aesar
Location		Wyoming, USA	Almeria, Spain	Černý vrch, Czech Republic	Milos, Greece	Bavaria, Germany	Lieskovec, Slovakia		
Corrosion tests	5	x	x	x	x	x	x		
Months	12	x	x	x	x	x	x		
	36	x	x	x	x	x	x		
Mineralogical composition (mass%) from Kaufhold et al. *(2012), B72 data based on methods described by Kaufhold* et al. *(2012)*									
Smectite		88	75	74	91	61	75		
Muscovite/illite			4			17			
Quartz		3	10	3		13	11		
Cristobalite		1					3		
Rutile/anatase				5	1		0		
Kaolinite				15		4	2		
Feldspar		7	8		8	5	8		
Calcite		1	3	2	0	0			
Gypsum		0							
Others (traces)				1			1		
Opal-A								100	
α-iron	[mass%]								> 99.5
Chemical composition (mass%) from Kaufhold et al. *(2008a), B72 data based on methods described by Kaufhold* et al. *(2008a)*									
SiO_2		58.6	54.1	45.0	52.8	55.0	61.7	91.0	
TiO_2		0.1	0.2	4.2	0.7	0.5	0.8	0.0	
Al_2O_3		19.5	15.5	15.4	18.0	18.1	17.5	0.3	
Fe_2O_3		3.6	3.4	13.8	3.4	5.8	8.1	0.1	
MnO		0.0	0.0	0.2	0.0	0.0	0.1	<0.001	
MgO		2.4	4.3	2.1	3.5	2.3	1.6	0.1	
CaO		1.2	2.9	1.0	1.5	1.2	1.3	0.2	
Na_2O		2.1	1.2	<0.01	0.5	0.3	0.4	0.1	
K_2O		0.5	1.2	0.0	0.5	1.7	1.4	0.0	
P_2O_5		0.0	0.1	0.1	0.2	0.1	0.1	0.0	
LOI		11.4	16.7	17.7	18.7	14.8	6.7	8.3	
Sum		99.7	99.7	99.6	99.7	99.7	99.7	99.9	

(*Continued*)

https://doi.org/10.1180/clm.2025.10018 Published online by Cambridge University Press

Table 1. (*Continued.*)

	B33, MX80	B19, FEBEX	B72, BCV	B6	B25	B36	Opal-A, silica gel, cat litter	Fe^0, iron, Alfa Aesar
C/S analysis (LECO; mass%) from Kaufhold et al. *(2008b), B72 data based on methods described by Kaufhold* et al. *(2008b)*								
C_{total}	0.1	0.4	0.3	0.0	0.1	0.1		
$C_{organic}$	0.1	0.0	0.2	0.0	0.1	0.1		
$C_{inorganic}$	0.1	0.3	0.1	0.0	0.0	0.0		
S_{total}	0.0	0.0	ND	0.0	0.0	0.0		
CEC and exchangeable cations (meg 100 g^{-1}) from Kaufhold et al. *(2008a), B72 data based in methods described by Kaufhold* et al. *(2008a)*								
CEC	82	83	65	107	63	56	8	
Na^+	57	20	ND	17	0	0		
K^+	2	3	ND	2	2	2		
Mg^{2+}	5	33	ND	36	15	17		
Ca^{2+}	33	47	ND	52	41	36		
Additional parameters								
LCD (eq/FU)	0.25	0.35	0.20	0.33	0.30	0.20		
SSS (mass%)	2.4	1.1	0.4	0.6	0.5	0.5	90	
Fe content in 6 g 1:1 Fe^0 mix (g)	3.1	3.1	3.3	3.1	3.1	3.2		
Fe content in 1:1 Fe^0 mix (mass%)	51.3	51.2	54.8	51.2	52.0	52.8		
Initial Fe^0/Fe ratio (%)	98	98	91	98	96	95		

eq/FU = equivalent per formula unit; ND = not determined.

Table 2. Overview of the reaction conditions of all iron/bentonite mixture experiments. Double 'x' entries mean that the samples were prepared as duplicates to investigate reproducibility.

	Corrosion tests at 23°C							
Sample	5 months	12 months	36 months	Opal-A added	60°C, 12 months	Na-exchanged	Water content	Iron particle size
B33	x	x	x		x			x
B19	x	x x	x					
B72	x	x x	x					
B6	x	x x	x	x	x	x	x	x
B25	x	x	x		x			x
B36	x	x	x	x	x	x	x	x

study, however, is to investigate iron/bentonite interactions. Iron of comparable purity was therefore used. In contrast, carbon steel contains some carbon, which may play a role with respect to corrosion. Kaufhold *et al.* (2025) compared various types of steels with different C contents and could not identify significant differences. Before trying to understand the role of admixtures, it was decided to focus on pure iron. As the reaction of pure iron with bentonite is already understood, further research should be performed on the role of relevant admixtures such as carbon. In the present study, however, pure iron was used. Four bentonites were selected and reacted with iron powder at both 23°C and 60°C in a glovebox to study the possible effects of temperature on the extent of corrosion. Similarly, for selected samples the water content (solid/liquid ratio) was varied in a separate series (6 g solid + 4 mL H_2O = 1.5; 6 g solid + 8 mL H_2O = 0.7), and the effect of the type of interlayer cation was studied using two natural Ca/Mg-bentonites before and after Na exchange. In addition, the effect of the presence of reactive silica (opal-A) was studied by comparing two bentonite/iron mixtures without addition of opal-A and with the addition of 100 mg opal-A corresponding to 3.0 mass% in the bentonite, which represents opal-A-rich bentonites, and 1.7 mass% in the bentonite/iron mixture. In another test series, the iron powder was classified into >100 and <100 μm fractions (using a sieve) to investigate the effects of particle size on corrosion.

All mixtures were placed in 25 mL Teflon vessels, sealed and shaken for 24 h in an end-over-end shaker to produce a homogeneous mixture. The vessels were transferred to a glovebox, and these were purged with nitrogen, opened and left standing for 2 weeks inside the glovebox (to remove the remaining oxygen in the mixture). Afterwards, 6 mL of degassed and deionized water was added to each vessel, and the vessels were sealed carefully. To investigate the evolution of the alteration phases, three equivalent samples were prepared and reacted for 5, 12 and 36 months, respectively. After the respective reaction time, the vessels were opened and dried inside the glovebox at 23°C for 1–2 weeks. Then they were ground outside the glovebox and split for further analysis. One part of the sample was sent out for Mössbauer analysis. The other part was analysed using XRD and simultaneous thermal analysis (STA).

A Zeiss Sigma 300 VP field emission gun (FEG) scanning electron microscope (SEM) was used to evaluate the homogeneity of the iron/bentonite mixtures and particle sizes of the Fe^0 particles. Images were recorded using a high-definition backscattered electron detector (HDBSD) at 20 kV (Fig. S2).

The run products were denoted according to their initial sample (e.g. B6 and the time of reaction; i.e. B6 12M). In case of variations from standard corrosion test conditions, additional information is provided. All corrosion tests conducted are summarized in Table 2.

Methods

The Mössbauer measurements were carried out with a modified transmission Mössbauer spectrometer produced by Wissenschaftliche Elektronik GmbH Starnberg/Germany (WissEl) using a self-built drive control and data acquisition unit at 77 and 298 K. Measurements were, however, all conducted at 298 K. The detectors were a proportional counter as well as a Si positive intrinsic negative (PIN) photodiode. ^{57}Co embedded in a rhodium matrix served as the gamma-radiation source. For cooling, the samples were placed on a self-built cryostat and cooled with liquid nitrogen. The data were fitted according to a least-squares method using Lorentzian-shaped lines with *Recoil Mössbauer Analysis* software. All isomer shift values are given relative to α-iron. Fe^{2+}/Fe^{3+} ratios obtained on the precursor materials (bentonite before the corrosion tests) were compared with ratios measured in a different Mössbauer laboratory (Chiou *et al.*, 2025). The difference in the values was 0.3 mass% on average.

Thermoanalytical investigations were performed using a Netzsch 449 F3 Jupiter thermobalance equipped with a differential scanning calorimetry/thermogravimetry (DSC/TG) sample holder linked to a Netzsch QMS 403 C Aeolus mass spectrometer (MS). A total of 100 mg of powdered material previously equilibrated at 53% relative humidity (RH) was heated from 25°C to 1150°C with a heating rate of 10°C min^{-1}. The devices were manufactured by Netzsch (Germany). TG patterns were evaluated with respect to the mass increase caused by the oxidation of iron, which can be used to determine the amount of remaining Iron.

XRD traces were recorded using a PANalytical X'Pert Pro θ-θ materials powder diffractometer (MPD; Co-*K*α radiation generated at 40 kV and 40 mA), equipped with a variable divergence slit (20 mm irradiated length), primary and secondary soller, diffracted beam monochromator, point detector and sample changer (sample diameter: 28 mm). The samples were investigated from 3°2θ to 80°2θ with a step size of 0.03°2θ and a measuring time of 10 s per step. For specimen preparation, the back-loading technique was used to minimize preferred orientation. Co-*K*α radiation was used to effectively minimize fluorescence from Fe, which can otherwise obscure diffraction peaks and reduce data quality.

Results and discussion

Mössbauer spectroscopy

All reacted samples were analysed by Mössbauer spectroscopy. Figure 2a shows a measured Mössbauer spectrum of native iron and the red reference spectrum used to fit the measured data. The 1:1 mixture of iron powder and bentonite sample B72, which in its natural pure state (before mixing with Fe powder) contained

https://doi.org/10.1180/clm.2025.10018 Published online by Cambridge University Press

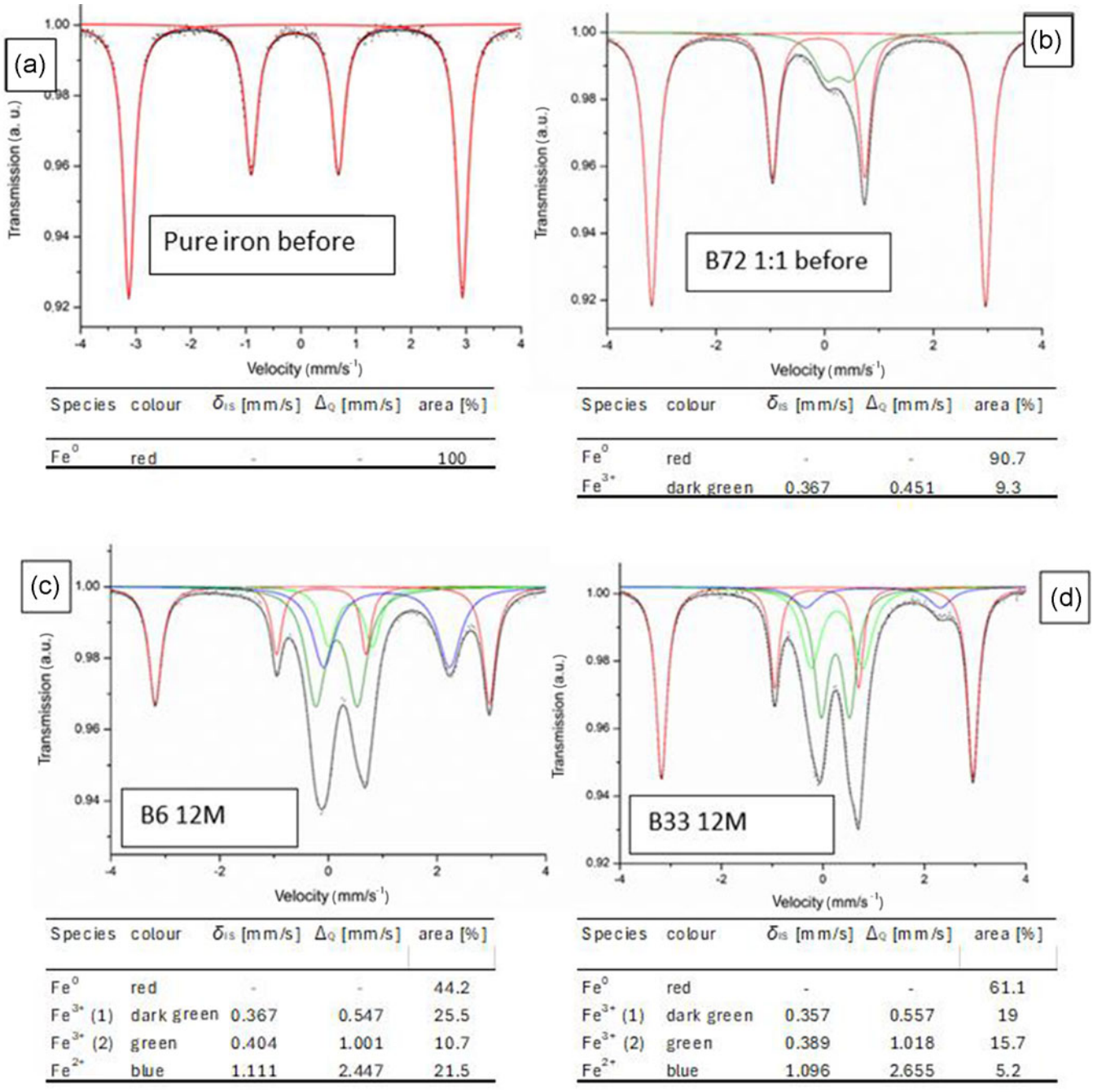


Figure 2. Mössbauer spectra of (a) unreacted iron, (b) iron powder/bentonite B72 mixture before the reaction, (c) reacted sample B6 12M and (d) sample B33 12M (d).

the most iron, was also investigated by Mössbauer spectroscopy for the characterization of the starting mixtures (Fig. 2b). The calculated content of native iron (Fe^0) was 91 mass% because of 9 mass% Fe contained in the bentonite (Table 1). The measured content of native iron was 90.7 mass%, corresponding to 9.3 mass% non-metallic Fe in the mixture before the reaction (Fig. 2b). The results of Mössbauer spectroscopy of selected representative samples (run products of B6 and B33 after 12 months) are shown in Fig. 2c,d. The most important difference between these samples is the intensity of the peaks fitted in red (representing pure iron) compared to the peaks fitted in blue and green (representing the sum of oxidized iron and octahedral iron initially present in the bentonite). The aim was to collect data to accurately assess the extent of oxidation of the native iron for which room-temperature Mössbauer measurements and fitting of the spectra using Fe^0, Fe^{3+} and Fe^{2+} references were applicable. The resulting ratio of the area of Fe^0 compared to Fe^{3+} and Fe^{2+} actually represents the ratio of iron to oxidized iron species. An example for the assessment of the extent of corrosion using this ratio is given in Fig. 2c,d. From the more intense red peak (Fe^0) of sample B33 (Fig. 2b) it is evident that this sample showed less corrosion compared to B6 (Fig. 2a) because more iron (Fe^0) was found after 12 months of reaction time.

https://doi.org/10.1180/clm.2025.10018 Published online by Cambridge University Press

Kaufhold *et al.* (2020a) used the Fe^{2+} value derived from Mössbauer spectroscopy for interpretation because in this test series the iron pellets were removed from the gel in the glovebox (iron pellets were picked out from the glovebox) and the samples were sealed in the glovebox and were not opened for Mössbauer spectroscopy (no reoxidation). In the present study, however, homogenization by grinding was required because the samples had to be split for the various analyses. The samples, therefore, had to be dried before grinding, which was done in the glovebox by ventilation with dry air. As an elevated temperature could not be used for more intense drying, it is suspected that in some samples the water content was not low enough to fully prevent reoxidation of Fe^{2+}, although the samples were dry enough for grinding. Native iron, on the other hand, is not as sensitive to oxidation as Fe^{2+} in reduced smectites and hence does not oxidize further in the dry state.

The spectra were fitted using iron (Fe^0), Fe^{2+} and two Fe^{3+} reference spectra, which enabled the determination of the relative abundances of iron oxidation states. The relative content of native iron turned out to be the most valuable parameter because it was barely affected by sample treatment after termination of the experiment (in contrast to the Fe^{2+}/Fe^{3+} ratio). The type and amount of corrosion products could not be fitted well in all Mössbauer spectra because of the lack of suitable references (mainly iron silicates), but the method turned out to be suitable for determining the amounts of the various oxidation states of the iron.

Evaluation of the extent of corrosion

In a starting mixture of iron-poor bentonite and native iron (before adding water), the content of iron determined by Mössbauer spectroscopy hence would be 100% regardless of the bentonite/iron ratio. Most of the bentonites, however, contain some iron, predominantly as Fe^{3+} (Chiou *et al.*, 2025), either as structural Fe in the smectite 2:1 framework or also in trace phases such as Fe-oxyhydroxides. The content of native iron in the starting 1:1 mixtures was, therefore, slightly below 100%. The initial Fe^0/Fe_{total} ratios of all bentonites are given in Table 1. As an example, sample B33 contains 3.6 mass% Fe_2O_3, corresponding to 2.5 mass% Fe. The total Fe content in a mixture of 3 g Fe^0 and 3 g B33 is, therefore, ∼51%, and the initial Fe^0/Fe ratio amounts to 98%. Notably, the total amount of Fe in the sample did not change throughout the experiments, but the portion of Fe^0 referred to as 'total Fe' decreased in the reacted samples according to the extent of corrosion (oxidation of iron). The Fe^0/Fe_{total} ratio (Fe^0/Fe ratio) in the run products depended on the extent of corrosion in such a way that corrosive bentonites led to lower iron ratios. Consequently, a bentonite/iron mixture with an iron ratio of 70% in the reaction product contained a bentonite that was less corroding compared to another bentonite of a bentonite/iron mixture in which an iron ratio of 50% was found. The relative amounts of Fe^{2+} and Fe^{3+} were not significant because these also depended on the post-experimental sample treatments (drying and grinding), which, for practical reasons, were done under oxic conditions (as explained earlier). The only Mössbauer parameter used for assessing the extent of corrosion, therefore, was the iron ratio (Fe^0/Fe_{total} = Fe^0/Fe ratio). Three samples were selected to test the reproducibility of the entire procedure, including the mixing of bentonite and iron (Fig. 3a). Deviations between the duplicates were <1%. The method is, therefore, suitable to assess the extent of iron corrosion induced by various bentonites. Based on this finding, differences in the iron ratio of >1% are considered significant.

The extent of corrosion was also determined by measuring the mass gains between 500°C and 1100°C using thermogravimetry (TG). The values were used to check the plausibility of the iron ratios determined by Mössbauer spectroscopy and to test a different method for assessing the extent of corrosion based on more rapid measurements. The TG mass gain is based on the fact that the iron powder increases in weight as a result of oxidation during TG measurement. An example is shown in Fig. 4. The grey curve in Fig. 4 represents pure iron (same powder as was used in the corrosion tests), which shows a mass gain of 34%. The blue curve in Fig. 4 represents the TG curve of sample B72 before mixing with iron powder. The extent of corrosion, however, was estimated based on comparing the mass gain of the unreacted and reacted mixtures. The mass gain of the pure iron was 34%, which would correspond to 17% in a 1:1 mixture. The red curve in Fig. 4 represents a real 1:1 mixture before reaction with water showing a mass gain of 16.9%, which is reasonably close to the theoretical value of 17%. The green curve in Fig. 4 represents the TG curve of the sample mass of the B72/iron mixture after 12 months (B72 12M) of reaction time (with water at 60°C). The TG mass gain was 4 mass% lower, which, when compared to the 100% sample, can be calculated as an iron ratio of ∼25%. Correlation of the results using parallel measurements of 20 samples using the Mössbauer and TG methods (Fig. 4b) indicates that both methods provide comparable results. As expected from such different and independent methods, the scatter is relatively large. This can possibly be explained by incomplete iron oxidation (thermal analysis) and the effect of varying $Fe^{2+/3+}$ ratios, which are affected by the post-corrosion sample treatment (as explained earlier) because oxidation of Fe^{2+} also leads to some mass gain. In addition, an overlapping of dehydroxylation mass loss of samples at higher dehydroxylation temperatures with starting mass gain at ∼600°C may explain some of this scatter, although the baseline for each different raw material was set individually. In the present study, Mössbauer spectroscopy was, therefore, preferred over the TG method to quantify the extents of corrosion of the various tests.

Size of Fe particles

Reactions taking place at interfaces are usually determined by the reactive surface area. Accordingly, it was assumed that the size of the iron particles would affect the results. A test series was set up to systematically investigate this effect. The original iron powder was dry sieved (steel sieve) to <100 and >100 µm fractions. SEM investigation proved the presence of a particle-size range from ∼20 to 200 µm (Fig. S2). The two grain-size fractions, therefore, could be referred to as the 20–100 and 100–200 µm fractions. Each of the fractions was mixed with four different bentonites and allowed to react for 12 months. The iron ratio (extent of corrosion) obviously was independent on the particle size tested (Fig. 5), which may provide valuable information with respect to the corrosion extent determining step. The results can possibly be explained by the following model: based on the reaction scheme provided by Kaufhold *et al.* (2015) – which was also explained earlier – the reduction of the structural Fe^{3+} of the smectite in the bentonite is supposed to play a crucial role with respect to the proceeding corrosion. The structural Fe^{3+} of the smectite can be reduced by the hydrogen dissolved in the water. The water, in turn, is supposed to be rich in dissolved H_2, and the extent of the reaction would depend on the reducibility of the smectite rather than the surface area of the iron. The hypothesis is that both sizes of iron particles in the tests would be small enough to provide excess H_2 anywhere in the system, which, of course, would not be the case if

https://doi.org/10.1180/clm.2025.10018 Published online by Cambridge University Press

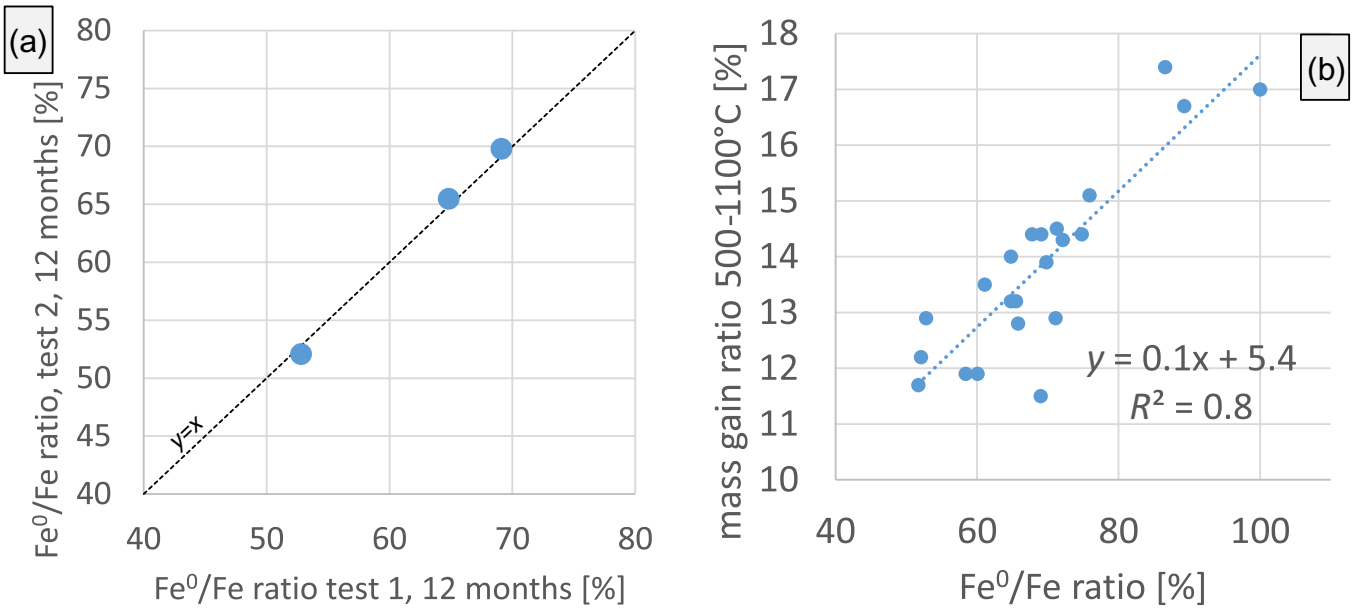


Figure 3. (a) Reproducibility test of Mössbauer spectroscopy for the investigation of bentonite/iron mixtures. The results are based on six different bentonite/iron mixtures prepared with three different bentonites representing the reproducibility of the entire procedure, including mixing, through termination of the reaction and up to Mössbauer analysis of the iron ratio. (b) Comparison of the iron ratios of 20 reacted samples through the mass gain ratio (thermogravimetry) caused by oxidation of native iron (and Fe^{2+}).

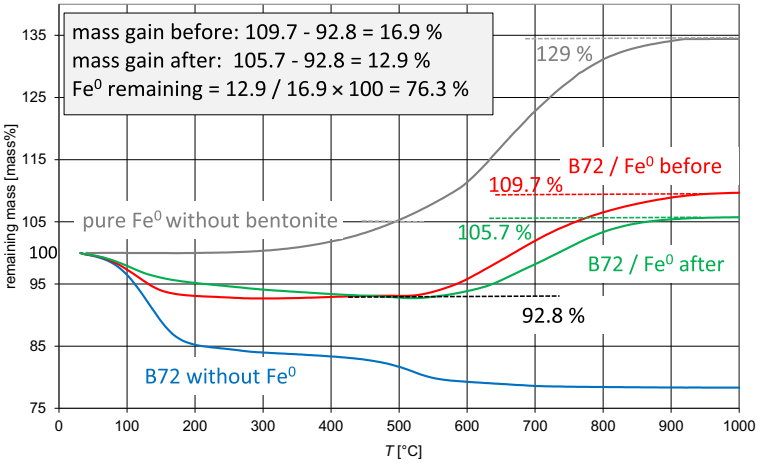


Figure 4. TG curves of native iron (grey), sample B72 (blue), sample B72 mixed with iron powder without addition of water (1:1; red = before) and sample B72 mixed with Fe powder after the reaction (B72 12M; green = after).

– as an extreme example – only one big iron pellet had been used. According to this model, corrosion would proceed as long as H_2 is consumed by reduction of the structural Fe^{3+} of the smectite. This possible explanation is a model that is in accordance with the corrosion mechanism proposed earlier, but it needs further systematic investigation.

Effect of the type of dominating exchangeable cations

Controversial results have been published with respect to the effect of the type of exchangeable cation on the corrosion rate or extent of corrosion (discussed earlier). In the present study, therefore, a different setup compared to Kaufhold *et al.* (2015) and Lantenois *et al.* (2005) was used to obtain additional information regarding the possible effect of exchangeable cations. Two bentonites were selected, of which B6 had been shown to be less corroding than B36 in most previous tests (Kaufhold *et al.*, 2015). These tests were based on gravimetrical measurements using iron pellets. Using a similar interlayer population, either natural Ca^{2+}/Mg^{2+}- or Na^{+}-exchanged, it was found that the LCD correlates with the extent of corrosion (Kaufhold *et al.*, 2015). In the present study, both bentonites were also used in their natural state (Ca^{2+}/Mg^{2+}) and after saturation with Na^{+}. The results of these corrosion tests are shown in Fig. 6. As expected, the mixture of iron and higher-charged bentonite B6 showed less corrosion both in the natural state (Ca^{2+}/Mg^{2+}) and in the Na^{+}-exchanged state after 12 months. The effect of the type of exchangeable cation, however, was more significant. Both mixtures of iron and natural Ca^{2+}/Mg^{2+} bentonites showed 61–65% iron ratios, but in case of the Na^{+}-exchanged bentonites more iron was preserved (iron ratio = 72–75%), and hence less corrosion. The results presented in Fig. 6 are consistent with those of Kaufhold *et al.* (2015), who stated that Na^{+} in the interlayer region leads to less corrosion if the other relevant parameters are held constant.

https://doi.org/10.1180/clm.2025.10018 Published online by Cambridge University Press

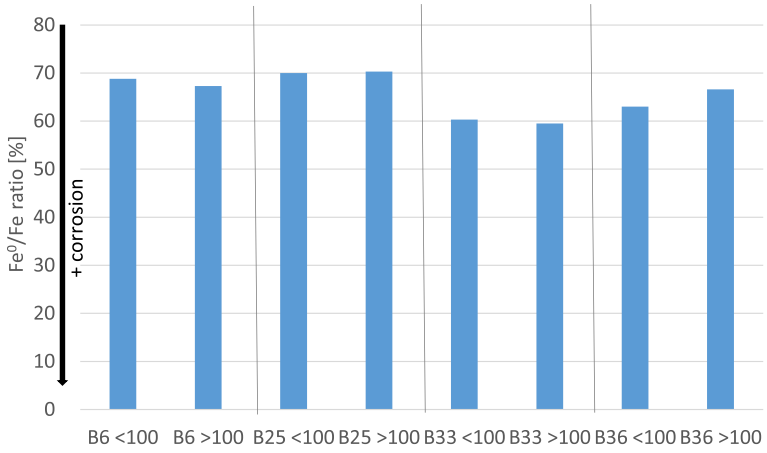


Figure 5. Comparison of the extent of iron corrosion (Fe^0/Fe ratio) of bentonites mixed variously sized iron powders. Tests were run for 12 months at room temperature. <100 = particles smaller than 100 µm; >100 = particles larger than 100 µm.

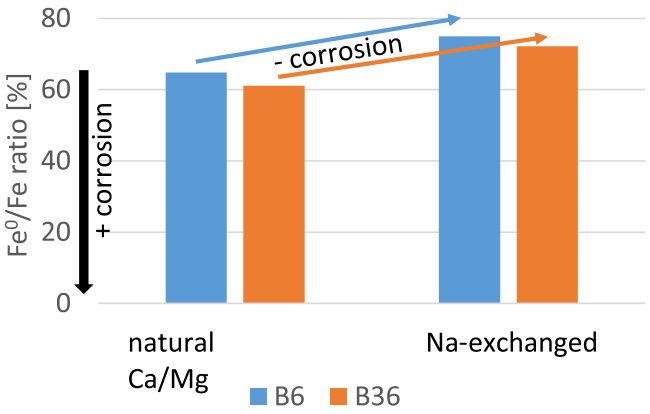


Figure 6. Comparison of the extent of corrosion of two natural Ca/Mg-bentonites before and after exchange with Na.

The run products (reacted mixtures) were analysed using XRD (Fig. 7). The most significant difference between the Ca/Mg- and the Na-exchanged iron bentonite mixtures was observed with respect to the 7 Å phase. Bentonite B6 did not contain any 7 Å phase before treatment, but a small reflection was detected for B36 (Fig. 7). For both natural Ca/Mg-rich samples, however, a significant increase in intensity at 7 Å was observed, but for the Na-exchanged B6 sample no indications of the formation of a 7 Å phase were found. The 7 Å intensity of the Na-exchanged sample B36, on the other hand, may be slightly larger compared to the precursor, but the 7 Å intensity of the Ca/Mg sample B36 showed a significant increase. The type of exchangeable cation obviously did not only affect the extent of corrosion, but also the type of corrosion product. In addition, lepidocrocite was found only in the Na-exchanged samples (Fig. 7). Lepidocrocite, however, may have formed during grinding or drying outside the glovebox because it forms under oxic conditions and hence was probably not a primary corrosion product. Samples were stored in the glovebox until they appeared to be dry. However, Na-exchanged bentonites, even in mixtures with iron, have a higher water content after drying under ambient conditions, which could have resulted in the oxidation of ferrous hydroxide. In the case of sample B6 Ca/Mg 12M, a peak was observed at ~5 Å, which could be assigned to the 003 reflection.

To date, it is not clear why Na- and Ca/Mg-bentonites show different corrosion rates. However, the fact that different corrosion products form depending on the exchangeable cation could be important in this respect. The corrosion rate could possibly be affected by the formation energies of the various corrosion products. However, the reason why different reactions take place remains to be investigated in future because the data provided in the present study do not allow us to draw any unambiguous conclusions on this matter.

Reactive silica

Kaufhold *et al.* (2020b) found that the presence or absence of reactive silica affected the corrosion reactions, at least at the beginning. The presence of reactive silica (defined as SSS) led to the immediate formation of Fe-silicates and hence less Fe-oxyhydroxide (ferrous hydroxide – magnetite). In that study, however, only different reaction pathways or mechanisms were identified, and it was not possible to conclude whether the presence of reactive silica accelerated corrosion, increased the extent of corrosion or vice versa. The experimental setup used in the present study, however, was suitable for investigating the effects of the presence or absence of reactive silica on the extent of corrosion. Therefore, two bentonites were selected: the less corroding B6 and the comparably corrosive B36. Both were mixed with the iron powder and both with and without addition of 1.7 mass% opal-A. The results are shown in Fig. 8. Both bentonites mixed with opal-A contained less iron after 12 months, which indicates that the reactive silica increased the extent of corrosion.

No significant differences in the XRD traces of iron and bentonite B36 mixtures with and without opal-A were observed (Fig. 9), which indicates that opal-A did not significantly affect the formation of corrosion products. This bentonite contained minor kaolinite before treatment. B6, on the other hand, which did not contain any kaolinite (initially present 7 Å phase) before treatment, showed a different XRD trace. In case of both B6 12M products (with and without opal-A), a 7 Å phase formed regardless of the presence or absence of opal-A, but the peak shape was different depending on the presence or absence of opal-A. The product that contained opal-A showed a sharp and symmetric 7 Å peak, but the sample that did not contain opal-A showed a pronounced asymmetry with a shoulder towards higher *d*-values. This peak shape can be explained either by the presence of two different phases differing with respect to structural order and/or different hydration states. The different peak shape, however, indicates that at least slightly

https://doi.org/10.1180/clm.2025.10018 Published online by Cambridge University Press

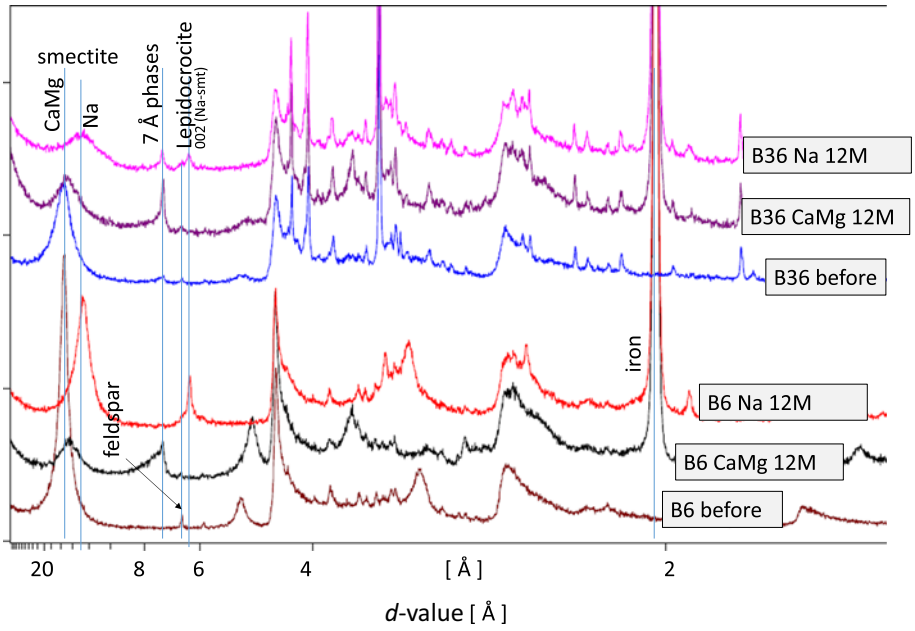


Figure 7. XRD traces of the run products of bentonites B6 and B36 (12 months) either with their natural cation population (Ca, Mg) or after Na exchange.

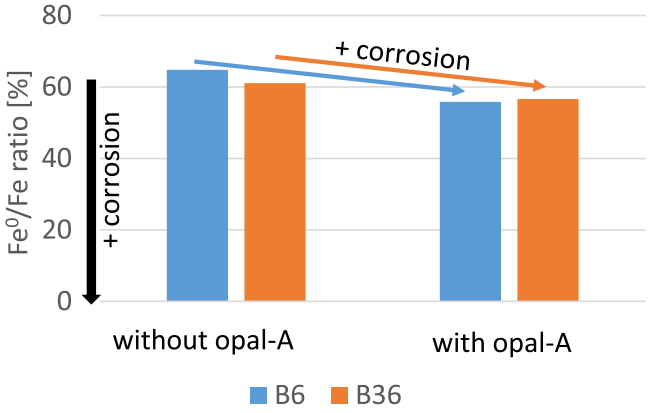


Figure 8. Comparison of the extent of corrosion of two bentonites with and without the addition of opal-A.

different siliceous corrosion products can form depending on the presence or absence of reactive silica.

Temperature

Temperature generally affects chemical reactions; typically, increasing temperature leads to an increase in the reaction rate. Hence, it was expected that corrosion would also depend on temperature. With respect to Fe corrosion while in contact with bentonite, Stoulil *et al.* (2013), however, found a reduced extent of corrosion at higher temperatures, which they explained according to the presence of a denser magnetite layer that formed at higher temperatures and in turn limited Fe^{2+} diffusion through it. In the present study, four bentonites were selected and reacted with iron powder at both 23°C and 60°C in a glovebox. The results are presented in Fig. 10. Mixtures of iron and bentonites B6, B25 and B36 all showed less corrosion at 60°C compared to at 23°C hence confirming the results published by Stoulil *et al.* (2013). The mixture of iron and bentonite B33, however, showed the opposite effect: more preserved native iron at 23°C, corresponding to less corrosion compared with the 60°C sample. In contrast to the other bentonites, B33 is a natural Na-bentonite (interlayer dominated by Na^+), and it contains naturally present reactive silica (SSS; see Table 1). Either difference could be the reason for the differing temperature behaviour. Based on the results published by Stoulil *et al.* (2013) and Kaufhold *et al.* (2020b), this differing temperature behaviour of the iron/bentonite B33 mixture could possibly be explained by the presence of reactive silica. According to Kaufhold *et al.* (2020b), less magnetite forms if reactive silica is present from the beginning onwards. In that case, the previously discussed 7 Å phase formed probably from a ferrous hydroxide gel. The denser magnetite layer of high-temperature samples (Stoulil *et al.*, 2013) would not exist if magnetite would not form and consequently could not lead to limited Fe^{2+} diffusion, hence limiting corrosion. In the sample with a greater content of reactive silica, the 7 Å phase (iron silicate) would form from the beginning onwards, leading to a less dense magnetite layer (if present at all). Without the presence of the dense magnetite layer, the increasing dissolution of smectite caused by higher temperatures would lead to more silica being available in the system, hence increasing corrosion (as shown earlier).

The results presented in the present paper do not allow for an unambiguous conclusion to be drawn because only few samples and two different temperatures were investigated. In future, more experiments at various temperatures should be performed to determine whether corrosivity may correlate with the temperature dependence of H_2 solubility in water, which shows a minimum at ~60°C (Sonne-Hansen *et al.*, 1999).

The iron/bentonite mixtures reacted at different temperatures were also investigated using XRD. For reacted samples of B06, B25 and B33, no significant differences in the XRD traces could be observed, except for some lepidocrocite that was found in the sample B33 12M run at 60°C. Formation of lepidocrocite (as explained earlier) is not supposed to reflect systematic differences in the corrosion but an effect of different conditions throughout sample treatment after termination of the corrosion tests. Sample B36, which contained some kaolinite and hence some 7 Å intensity before treatment (Fig. 11), showed increased 7 Å intensity in the reacted samples and a slightly different intensity ratio

https://doi.org/10.1180/clm.2025.10018 Published online by Cambridge University Press

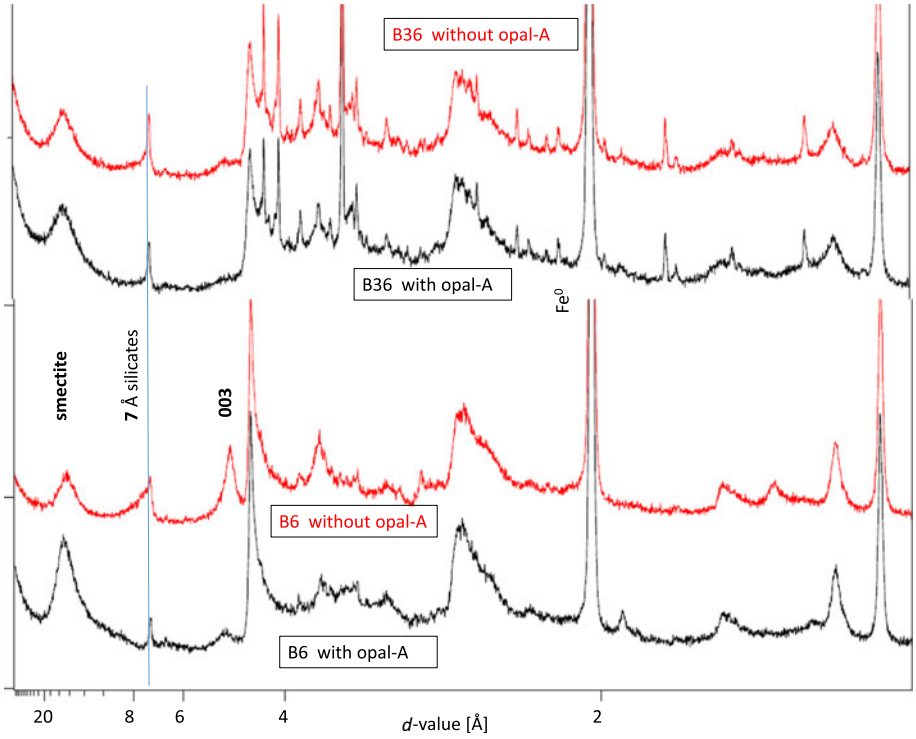


Figure 9. Comparison of XRD traces of bentonite/iron mixtures reacted for 12 months with and without the addition of opal-A.

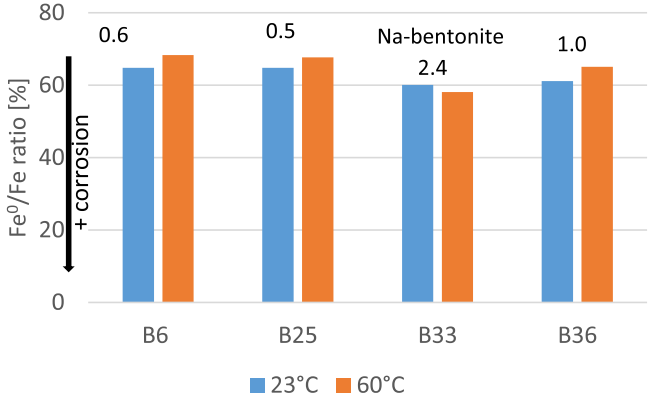


Figure 10. Extents of corrosion expressed as the iron ratios of four different iron/bentonite mixtures at two different temperatures. The numbers indicate the contents of naturally present reactive silica of the bentonites in mass%. B33 is the only natural Na^+-rich bentonite (61% Na^+; Table 1) used for preparing the iron/bentonite mixtures.

of the smectite d_{001} reflection and the 7 Å reflection (Fig. 11) at different temperatures. These differences, however, were too small to derive further unambiguous conclusions. More systematic work (more samples containing various exchangeable cations and various amounts of reactive silica) remains to be conducted to understand the effects of temperature on the type of corrosion product.

Water content

Water is assumed to play a key role in corrosion because it is supposedly needed for ion and (indirect) electron transfer (possibly *via* H_2 dissolved in water). Water, therefore, is a key reactant for the discussed reactions. Kaufhold *et al.* (2015) found that pure water (iron pellets in water without bentonite) was much less corroding compared to systems containing bentonite. Tests performed with bentonite and various water contents indicated that increasing water contents either did not significantly affect corrosion or caused a slight decrease in the corrosion rate. These tests were conducted using iron pellets. In the present study, iron powder was mixed with bentonite (1:1) and, for selected samples, the solid (bentonite + iron)/liquid (water) ratio was varied from 0.7 to 1.5. Lower solid/liquid ratios were not applicable because these mixtures were no longer in a gel state. The standard solid/liquid ratio in all other tests was 1 (3 g iron + 3 g bentonite + 6 mL water). The results shown in Fig. 12 indicate that lower or slightly higher solid/liquid ratios compared to reference conditions (solid/liquid ratio = 1) did not significantly affect the measured extents of corrosion. In an application such as a barrier with highly compacted bentonite in contact with an iron canister surface (shown as the grey-shaded range in Fig. 12), the compacted bentonite blocks may have water contents ranging from 10 to 40 mass%, and hence the water content will be lower compared to the water contents used in the present study (Fig. 12). The analytical setup, however, was chosen so as to use as little water as possible (and so to be as close to real conditions as possible) but as much water as was required for preparing homogeneous gels. The results presented in Fig. 12 indicate that small differences in the solid/liquid ratios either above or below the reference conditions did not systematically affect the extent of corrosion.

Comparison of bentonites

All bentonites were tested using standard conditions after 5, 12 and 36 months to gain information on the evolution of the corrosion extent over time. The results are shown in Fig. 13. As would be expected, corrosion was faster at the beginning, before slowing

https://doi.org/10.1180/clm.2025.10018 Published online by Cambridge University Press

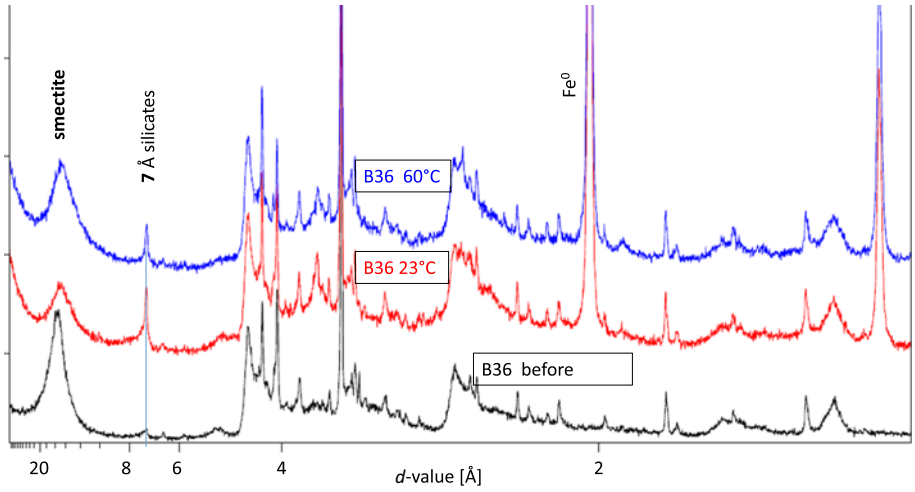


Figure 11. XRD traces of bentonite B36 before the corrosion tests (black) and of the iron/bentonite B36 mixtures reacted at two different temperatures (red = 23°C; blue = 60°C).

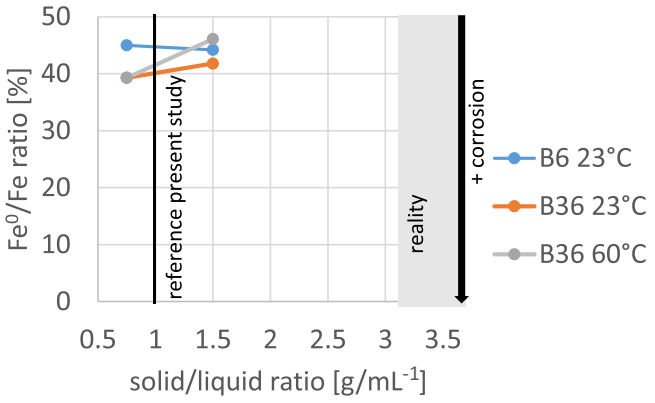


Figure 12. Extent of corrosion measured as the remaining iron ratio of two different bentonites depending on the solid/liquid ratio ranging from 0.7 (3 g iron powder + 3 g bentonite + 4 mL water) to 1.5 (6 g solid + 8 mL water). All mixtures were stable gels.

down after 5 months. The shapes of the curves (represented as lines between the measured values) prove that, for some samples, corrosion continued after 36 months (B6, B25, B72), and it reached a constant extent of corrosion after 12 months in case of the other samples (B33, B19, B36).

The lowest extent of corrosion was found for the iron/bentonite B19 mixture, and the iron/bentonite B72 mixture showed the greatest extent of corrosion (Fig. 13). The different extents of corrosion could depend on the smectite content (Fig. 14a). On average, lower extents of corrosion were found for samples with greater smectite contents, but the correlation between smectite content and extent of corrosion is poor (Fig. 14a) and hence does not allow us to conclude that there is an effect of smectite content on corrosivity. Instead, as has been reported previously (Kaufhold *et al.*, 2015), a good correlation between the LCD and extent of corrosion was observed (Fig. 14b). Even the naturally Na-rich iron bentonite mixture (Fe^0 + B33) did not deviate from this trend, as has been reported previously for some iron/Na-bentonite mixtures (Kaufhold *et al.*, 2015). The differing extents of corrosion caused by various bentonites in the iron/bentonite mixtures hence can be explained by the varying LCD of their smectites, as has been reported previously (Kaufhold *et al.*, 2015).

Summary and conclusions

Corrosion tests conducted with iron powders and bentonite powders mixed with water to achieve a gel state allowed us to investigate corrosion by analysing bulk samples, which is hardly possible when using pellets.

Mössbauer spectroscopy, thermal analysis and XRD were used for the investigation of corrosion. Quantitative values representing the extent of corrosion were obtained using Mössbauer spectroscopy based on the ratio of native iron that remained unreacted in the bentonite gel compared with total iron. Accordingly, low contents or ratios of native iron (referred to as 'total iron') in the run products corresponded to more intense corrosion. Quantification of the mass gain by TG resulting from oxidation of native iron was also tested for quantification of the remaining iron. This method, however, was less precise compared to Mössbauer spectroscopy.

XRD could not be used in a quantitative manner because of (1) the difficulty of describing the highly disordered structure of the corrosion products (including the 7 Å phase if present), (2) the possible presence of amorphous components (ferrous hydroxide and/or iron silicate gel) and (3) the presence of native iron, which significantly reduced XRD intensities (microabsorption). The XRD results could, however, be evaluated qualitatively. As an example, the XRD results indicated that the type of interlayer cation affected the type of corrosion product formed, which has not been reported previously. In the present study, formation of a 7 Å phase was only observed for Ca/Mg-bentonites and not after exchange for Na^+ in mixtures with iron. For the first time, we could prove that the type of exchangeable cation can affect the type of corrosion product. This could be an explanation for the fact that sometimes 7 Å phases have been reported in the literature and sometimes only magnetite. The reason for the effect of the type of exchangeable cation, however, could not be determined in this study. Notably, the type of exchangeable cation also affected the extent of corrosion of iron/bentonite mixtures, which was slightly lower in case of interlayer Na^+.

Temperature also affected the extent of corrosion. Three mixtures of iron and Ca/Mg-bentonite showed less corrosion at 60°C compared to at 23°C, but sample B33 (the only natural Na-bentonite and the only bentonite containing some naturally present reactive silica) showed the opposite trend in mixtures with iron. The number of samples investigated at various temperatures in the present study was too small compared to the number of variables

https://doi.org/10.1180/clm.2025.10018 Published online by Cambridge University Press

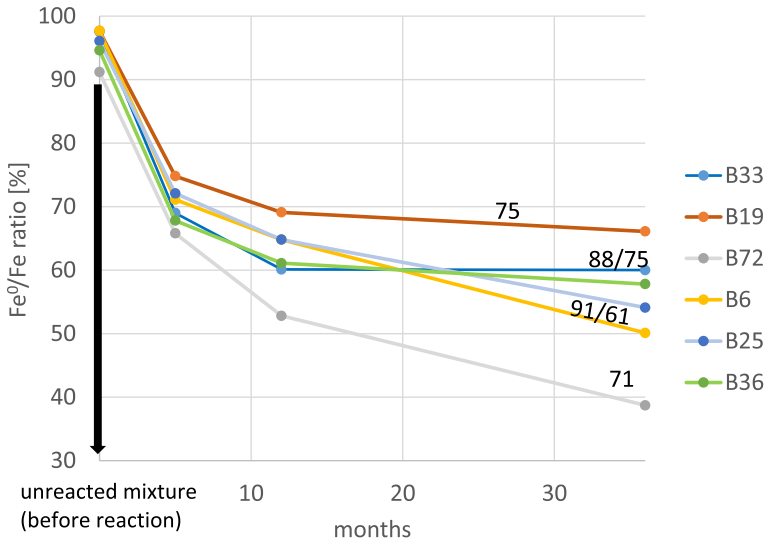


Figure 13. Evolution of the extent of corrosion determined based on the amount of remaining iron after the reaction over time (numbers indicate the smectite content in mass%) of the initial bentonites.

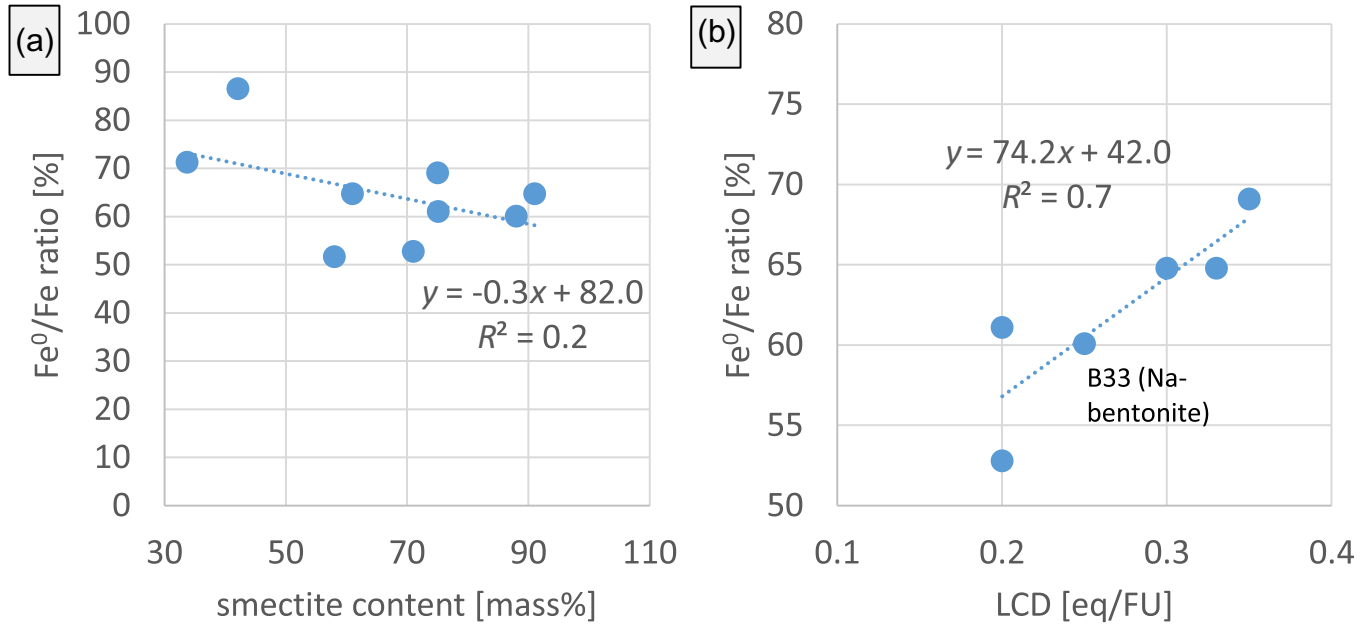


Figure 14. Comparison of the extents of corrosion after 12 months expressed as the iron ratio (a) with the smectite content of the bentonites in the iron/bentonite mixtures (Kaufhold *et al.*, 2012) and (b) with the LCD (given in equivalent per formula unit; eq/FU) of the smectites in the iron/bentonite mixtures.

(type of exchangeable cation and reactive silica) to draw any other conclusions than the fact that further studies are needed with more samples (different exchangeable cation and different amounts of reactive silica) and ideally a wider range of temperatures.

The variation in the particle size of the iron particles (<100 and >100 μm) did not significantly affect the extents of corrosion, which possibly can be understood based on the assumption that excess H_2 was present in both cases (small and larger iron particles). The corrosion rate hence would be determined by the reduction of the structural Fe^{3+} of smectites, which causes hydrogen consumption and the formation of iron phases such as silicates or oxides, but not by the particle size of the iron (as long as the iron particles provide an excess of H_2 everywhere in the system).

The presence or absence of reactive silica (opal-A) is known to affect corrosion (Rivard *et al.*, 2015; Kaufhold *et al.*, 2020b). The present study, however, for the first time proves that the presence of reactive silica not only affects the corrosion product but also increases the corrosion rate. Using opal-A-poor bentonites in combination with carbon steel, therefore, would increase HLRW canister lifetime. The effect of differing water contents, on the other hand, was low as long as the samples remained in a gel state.

Differing extents of corrosion caused by various bentonites in mixtures with iron were observed and could be explained by the differing layer-charge densities of their smectites. The trend observed corresponds to what has been reported previously (Kaufhold *et al.*, 2015) in that bentonites containing low-charged smectites were more corrosive, demonstrating a greater extent of corrosion (i.e. less remaining iron).

https://doi.org/10.1180/clm.2025.10018 Published online by Cambridge University Press

Tests run for 36 months proved that the corrosion of the bentonite/iron mixtures proceeded in differing manners. Three bentonite/iron mixtures did not react further after 12 months, and the other three samples showed ongoing corrosion past this duration. Such bentonites would, of course, be preferable barrier materials with the potential to substantially increase HLRW canister lifetime. Understanding the reasons for this differing behaviour, therefore, represents an important future challenge. The identification of the reasons as to why various bentonites show differing long-term behaviour is particularly important for the selection of an ideal bentonite/iron HLRW canister combination (with respect to the lifetime of the canister).

The results of the present study prove that various parameters affect both the extent of corrosion and the reaction, leading to differing corrosion products. To understand the iron/bentonite interface to a greater extent, particularly with respect to the possibility of predicting corrosion through modelling, further systematic investigations are needed that consider the type of exchangeable cation, the content of SSS and temperature. The water content and particle size (surface area) of the iron, on the other hand, are suggested to be less important in this regard. In addition, the separation of reacted and residual iron from the run products before analysis (e.g. by XRD) would be beneficial. Based on the results presented in this study, high-charged, SSS-free Na-bentonites are preferable with respect to the lifetime of a HLRW iron canister in a real repository because less corrosion can be expected with such a material.

Supplementary material. The supplementary material for this article can be found at https://doi.org/10.1180/clm.2025.10018.

Acknowledgements. Sven Krüger gratefully acknowledges the Leibniz Supercomputing Centre for supporting this project by providing computing time on its Linux-Cluster.

Financial support. This research was partially funded by the German Federal Ministry for the Environment, Climate Action, Nature Conservation and Nuclear Safety (BMUKN), project 02E11870D.

Competing interests. The authors declare none.

References

Battallion C., Bouchon F., Chainais-Hillairet C., Desgranges C., Hoarau E., Martin F. *et al.* (2010) Corrosion modelling of iron based alloy in nuclear waste repository. *Electrochimica Acta*, **55**, 4451–4467.

Bildstein O., Trotignon L., Perronnet M. & Jullien M. (2006) Modelling iron–clay interactions in deep geological disposal conditions. *Physics and Chemistry of the Earth, Parts A/B/C*, **31**, 618–625.

Červinka R., Večerník P., Kašpar V. & Vašíček R. (2018) *Kompletini charakterizace bentonite BCV 2017*. Technická zpráva číslo 419/2019. SÚRAO, Prague, Czech Republic, 39 pp.

Chiou W.-A., Dohrmann R., Kaufhold S., Plötze M., Stucki J.W. & Ufer K. (2025) Sample characterization. Pp. 39–144 in: *Bentonites – From Mine to Application* (S. Kaufhold, editor). Geologisches Jahrbuch B 107. Schweizerbart, Stuttgart, Germany.

Didier M., Leone L., Greneche J.-M., Giffaut E. & Charlet L. (2012) Adsorption of hydrogen gas and redox processes in clays. *Environmental Science and Technology*, **46**, 3574–3579.

Drits V.A. & Manceau A. (2000) A model for the mechanism of Fe^{3+} to Fe^{2+} reduction in dioctahedral smectites. *Clays and Clay Minerals*, **48**, 185–195.

El Mendili Y., Abdelouas A., Ait Chaou A., Bardeau J.-F. & Schlegel M.L. (2014) Carbon steel corrosion in clay-rich environment. *Corrosion Science*, **88**, 56–65.

Fernández A.M., Cuevas J. & Rivas P. (2001) Pore water chemistry of the FEBEX bentonite. *Materials Research Society Symposium Proceedings*, **663**, 573–588.

Fernández A.M., Kaufhold S., Sánchez-Ledesma D.M., Rey J.J., Melón A., Robredo L.M. *et al.* (2018) Evolution of the THC conditions in the FEBEX *in situ* test after 18 years of experiment: smectite crystallochemical modifications after interactions of the bentonite with a C-steel heater at 100 °C. *Applied Geochemistry*, **98**, 152–171.

Gorski C.A., Klüpfel L E., Voegelin A., Sander M. & Hofstetter T.B. (2013) Redox properties of structural Fe in clay minerals: 3. Relationships between smectite redox and structural properties. *Environmental Science and Technology*, **47**, 13477–13485.

Guillaume D., Neaman A., Cathelineau M., Mosser-Ruck R., Peiffert C., Abdelmoula M. *et al.* (2003) Experimental synthesis of chlorite from smectite at 300 °C in the presence of metallic Fe. *Clay Minerals*, **38**, 281–302.

Hausmannová L., Hanusová I. & Dohnálková M. (2018) *Summary of the Research of Czech Bentonites for Use in the Deep Geological Repository – Up to 2018*. Technical Report 309/2018/ENG. SÚRAO, Prague, Czech Republic, 64 pp.

Jacobsson A. & Pusch R. (1978) *Egenskaper hos bentonitbaserat buffertmaterial*. KBS Teknisk rapport 1978-06-10. KBS, Stockholm, Sweden, 159 pp.

Jaisi D.P., Kukkadapu R.K., Eberl D.D. & Dong H. (2005) Control of Fe(III) site occupancy on the rate and extent of microbial reduction of Fe(III) in nontronite. *Geochimica et Cosmochimica Acta*, **69**, 5429–5440.

Jullien M., Raynal J., Kohler E. & Bildstein O. (2005) Physicochemical reactivity in clay-rich materials: tools for safety assessment. *Oil & Gas Science and Technology – Revue d'IFP Energies nouvelles*, **60**, 107–120.

Kaufhold S. (editor) (2025) *Bentonites – From Mine to Application*. Geologisches Jahrbuch B 107. Schweizerbart, Stuttgart, Germany.

Kaufhold S., Dohrmann R., Koch D. & Houben G. (2008a) The pH of aqueous bentonite suspensions. *Clays and Clay Minerals*, **56**, 338–343.

Kaufhold S., Dohrmann R. & Ulrichs C. (2008b) Shelf life stability of diatomites. *Applied Clay Science*, **41**, 158–164.

Kaufhold S., Dohrmann R., Stucki J. & Anastácio A.S. (2011) Layer charge density of montmorillonite – closing the gap between structural formula method and alkyl ammonium method. *Clays and Clay Minerals*, **59**, 200–211.

Kaufhold S., Hein M., Dohrmann R. & Ufer K. (2012) Quantification of the mineralogical composition of clays using FTIR spectroscopy. *Journal of Vibrational Spectroscopy*, **59**, 29–39.

Kaufhold S., Sanders D., Dohrmann R. & Hassel A.-W. (2015) Fe corrosion in contact with bentonites. *Journal of Hazardous Materials*, **285**, 464–473.

Kaufhold S., Dohrmann R. & Gröger-Trampe J. (2017) Reaction of native copper in contact with pyrite and bentonite in anaerobic water at elevated temperature. *Corrosion Engineering Science and Technology*, **52**, 349–358.

Kaufhold S., Klimke S., Schlömer S., Alpermann T., Renz F. & Dohrmann R. (2020a) About the corrosion mechanism of metal iron in contact with bentonite. *Earth and Space Chemistry*, **4**, 711–721.

Kaufhold S., Schippers A., Marx A. & Dohrmann R. (2020b) SEM study of the early stages of Fe-bentonite corrosion – the role of naturally present reactive silica. *Corrosion Science*, **171**, 108716.

Kaufhold S., Dohrmann R. & Weber C. (2021) Evolution of the pH value at the iron–bentonite interface at low solid/liquid ratios. *Applied Clay Science*, **201**, 105929.

Kaufhold S., Dohrmann R., Ufer K., Gröger-Trampe J., Kober F., Schneeberger R. & Weber C. (2024) HotBENT experiment quality control of bentonites used for GBM backfilling and block production. *Clay Minerals*, **59**, 265–286.

Kaufhold S., Kahra C., Finck N., Hassel T. & Muñoz A.G. (2025) Comparison of the metal/bentonite interaction of six different potential HLRW canister materials under anaerobic conditions. *Journal of Nuclear Materials Management*, **52**, 4–15.

Kiczka M., Alt-Epping P., Hadi J., Wersin P., Leupin O.X. & Diomidis N. (2024). Reactive transport modelling of iron bentonite interaction in the FEBEX *in situ* experiment. *Applied Geochemistry*, **170**, 106057.

Kosec T., Qin Z., Chen J., Legat A. & Shoesmith D.W. (2015) Copper corrosion in bentonite/saline groundwater solution: effects of solution and bentonite chemistry. *Corrosion Science*, **90**, 248–258.

Lanson B., Lantenois S., van Aken P.A., Bauer A. & Plançon A. (2012) Experimental investigation of smectite interaction with metal iron at 80°C: structural characterization of newly formed Fe-rich phyllosilicates. *American Mineralogist*, **97**, 864–871.

Lantenois S., Lanson B., Muller F., Bauer A., Jullien M. & Planc A. (2005) Experimental study of smectite interaction with metal Fe at low temperature: 1. Smectite destabilization, *Clays and Clay Minerals*, **53**, 597–612.

Lee C.T., Qin Z., Odziemkowski M. & Shoesmith D.W. (2006) The influence of groundwater anions on the impendance behavior of carbon steel corroding under anoxic conditions. *Electrochimica Acta*, **51**, 1558–1568.

Martin F.A., Bataillone C. & Schlegel M.L. (2008) Corrosion of iron and low alloyed steel within a water saturated brick of clay under anaerobic deep geological disposal conditions: an integrated experiment, *Journal of Nuclear Materials*, **379**, 80–90.

Mota-Heredia C., Cuevas J., Ruiz A.I., Ortega A., Torres E., Turrero M.J. & Fernández R. (2023) Geochemical interactions at the steel–bentonite interface caused by a hydrothermal gradient. *Applied Clay Science*, **240**, 106984.

Neretnieks I. (1978) *Transport of Oxidants and Radionuclides through a Clay Barrier*. Kungl Tekniska Högskolan Stockholm 1978-02-20. KBS, Stockholm, Sweden, 43 pp.

Osacky M., Sucha V.A., Czímerová A. & Madejová J. (2010) Reaction of smectites with iron in nitrogen atmosphere at 75°C. *Applied Clay Science*, **50**, 237–244.

Perronnet M., Jullien M., Villiéras F., Raynal J., Bonnin D. & Bruno G. (2008) Evidence of a critical content in Fe^0 on FoCa7 bentonite reactivity at 80°C. *Applied Clay Science*, **38**, 187–202.

Pusch R. (2002) *The Buffer and Backfill Handbook. Part 2: Materials and Techniques*. SKB Technical Report TR-02-12. SKB, Stockholm, Sweden, 197 pp.

Rivard C., Pelletier M., Michau N., Razafitianamaharavo A., Abdelmoula M., Ghanbaja J. & Villieras F. (2015) Reactivity of Callovo–Oxfordian claystone and its clay fraction with metallurgic iron: role of non-clay minerals in the interaction mechanism, *Clays and Clay Minerals*, **63**, 290–310.

Romaine A., Sabot R., Jeannin M., Necib S. & Refait P.H. (2013) Electrochemical synthesis and characterization of corrosion products on carbon steel under argillite layers in carbonated media at 80°C. *Electrochimica Acta*, **114**, 152–158.

Savoye S., Legrand L., Sagon G., Lecomte S., Chausse A., Messina R. & Toulhoata P. (2001) Experimental investigations on iron corrosion products formed in bicarbonate/carbonate-containing solutions at 90°C. *Corrosion Science*, **43**, 2049–2064.

Schikorr G. (1933) The iron (II) hydroxide and a ferromagnetic iron (III) hydroxide. *Zeitschrift für anorganische und allgemeine Chemie*, **212**, 33–39.

Schlegel M.L., Necib S., Daumas S., Labat M., Blanc C., Foy E. & Linard Y. (2018) Corrosion at the carbon steel–clay borehole water interface under anoxic alkaline and fluctuating temperature conditions. *Corrosion Science*, **136**, 70–90.

Sellin P. & Leupin O.X. (2013) The use of clay as an engineered barrier in radioactive-waste management – a review. *Clays and Clay Minerals*, **61**, 477–498.

Sonne-Hansen J., Westermann P. & Ahring B.K. (1999) Kinetics of sulfate and hydrogen uptake by the thermophilic sulfate-reducing bacteria *Thermodesulfobacterium* sp. strain JSP and *Thermodesulfovibrio* sp. strain R1Ha3. *Applied and Environmental Microbiology*, **65**, 1304–1307.

Stoulil J., Kanok J., Kouril M., Parschova H. & Novak P. (2013) Influence of temperature on corrosion rate and porosity of corrosion products of carbon steel in anoxic bentonite environment. *Journal of Nuclear Materials*, **443**, 20–25.

Sun Y., Zhou Y., Wei X., Dong J., Chen N., Ren Q. *et al.* (2023) Effects of iron corrosion products on the degradation of bentonite structure and properties. *Materials Degradation*, **7**, 66.

Wilson J., Sasamoto H., Tachi Y. & Kawama D. (2025) A review on the effect of iron on bentonite stability. *Applied Clay Science*, **275**, 107862.

Zandanel A., Sauer K.B., Rock M., Caporuscio F.A. & Telfeyan K. (2022) Impacts of crystalline host rock on repository barrier materials at 250°C: hydrothermal co-alteration of Wyoming bentonite and steel in the presence of Grimsel granodiorite. *Minerals*, **2024**, 1556.

https://doi.org/10.1180/clm.2025.10018 Published online by Cambridge University Press